Current Science
CS 4 (5), 770– 780 (2024)
Received 20 **July** 2024 | **Revised** 25 **August** 2024 | **Accepted** 25 Sept. 2024 | **Online Available** 30 **October** 2024
https://doi.org/10.52845/CS/2024-4-5-11

Current Science

Current Science

OPEN ACCESS

ISSN (O) 2795-8639

ORIGINAL ARTICLE

Torsional Vibration Optimization Design of Fracturing Truck Transmission Shaft Based on Improved Ant Colony Algorithm

Yuan Liang [a], Shuo Zhao[a], Liping Tan[b*], Hongyan Wang[c*], Chengzhi Xue[d], Yunteng Ma[e], Linchuan Zhang[e], Haoyu Guo[e]

[A]College of Mechanical and Electrical Engineering, China University of Petroleum (East China), & China National Engineering Research Center of Marine Geophysical Prospecting and Exploration and Development Equipment, China University of Petroleum (East China), Qingdao 266580, China

[B]Ulsan Ship and Ocean College Ludong University, Yantan, China

[c]College of Electromechanical Engineering, Qingdao University of Science & Technology, Qingdao 266061, China

[D]Xuzhou Construction Machinery Group, Xuzhou 221004, China

[E]Weichai Power Co., Ltd., Weifang 261061, China

Corresponding Author: Liping Tan and Hongyan Wang

Abstract:
Torsional vibration of the transmission system on the fracturing truck is an important factor triggering the vibration of the whole equipment. In this study, the sensitivity analysis of the total parameter model of the transmission system is conducted to find the structural parameters of the transmission system that have a greater influence on the response of torsional vibration. The ant colony optimization (ACO) algorithm is introduced into the continuous domain optimization problem by adding a coding disk, and the improved heuristic function is introduced. The improved ACO has better global search capability and convergence speed compared with the traditional algorithm. After 25 times of optimization search, the global optimal combination of optimized parameters is obtained, and the torsional vibration amplitude at the engine crankshaft output is reduced by 17.2%.
Keywords: Torsional vibration; Transmission system; Fracturing truck; Ant colony optimization algorithm

Introduction

Torsional vibration has always been a critical concern for the operation of the transmission system. The current research on torsional vibration control methods mainly focuses on frequency adjustment method to change the relevant parameters of the system and vibration energy reduction method to add vibration dampers. For devices with limited installation space, the frequency adjustment method is a preferable approach. The parameter optimization algorithms based on frequency adjustment method mainly include genetic algorithm (GA) [1], simulated annealing (SA) algorithm [2], particle swarm algorithm (PSO) [3], ant colony algorithm optimization (ACO) [4], etc. The ACO is a population-based heuristic bionic algorithm that employs a distributed positive feedback parallel computing mechanism, which is easy to combine with other methods and has strong robustness. The ACO is widely used in the field of discrete system optimization such as combinatorial optimization problem, such as reconfiguration of electrical networks [5], path planning problem [6], wireless sensor network (WSN) [7], graph coloring problem (GCP) [8], target tracking problem (TTP) [9] and pipe routing design (PRD) [11-12], etc.

However, in continuous domain optimization problems such as dimensional parameter optimization, the ACO suffers from the defects of difficult solution and low accuracy [13-20].

In this study, the ACO algorithm is purposefully improved and introduced into the continuous domain optimization problem to solve the engineering problem of structural optimization of the equipment transmission system on the fracturing truck platform.

The rest of this study is organized as follows: Section 2 presents the mathematical optimization model. Section 3 introduces the traditional ACO algorithm and the improved mechanisms. In Section 4, a set of experiments are conducted and results are analyzed. Finally, Section 5 introduces the conclusion.

2 Mathematical optimization model

2.1 Equipment transmission system on the fracturing truck platform

The transmission system of equipment on the fracturing truck generally consists of three components: the engine crankshaft system, the hydraulic transmission system and the reciprocating fracturing pump crankshaft system, and its simplified model is shown in Fig 1. The three main mechanisms of the transmission system are simplified based on the principles of simplification related to the aggregate parametric model, and the aggregate parametric models obtained are shown in Fig 2~Fig 4.

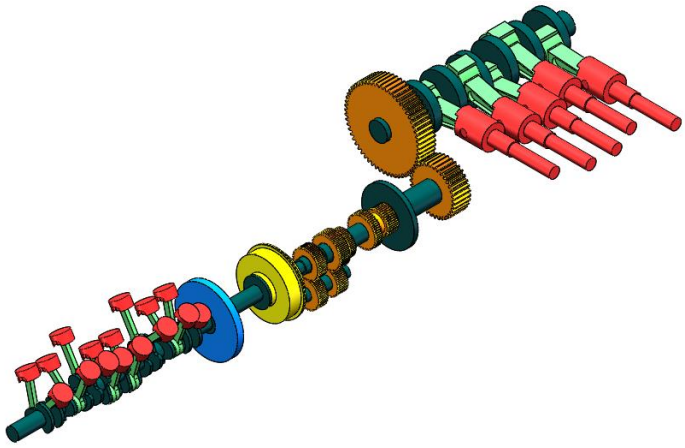

Figure 1 Transmission system model

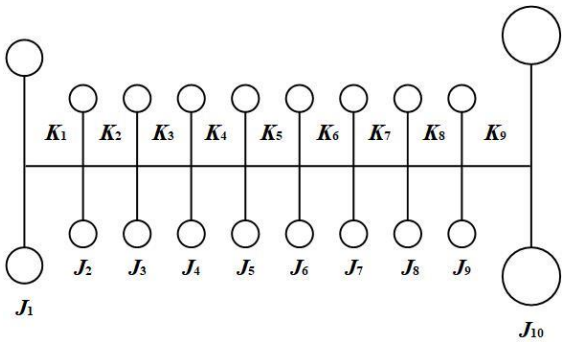

Figure 2 Diagram of engine crankshaft equivalent system

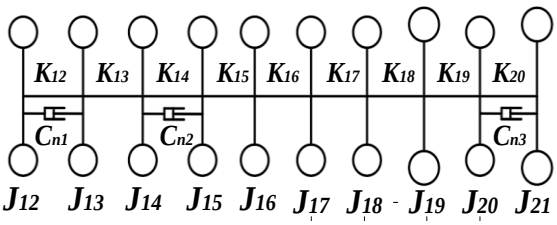

Figure 3 Parameter model of gear speed mechanism set

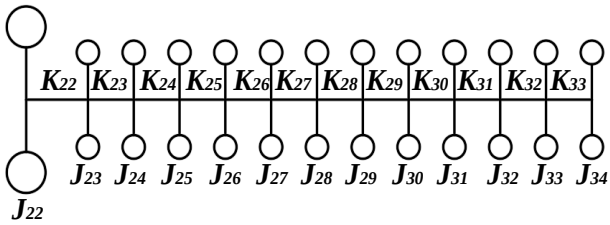

Figure 4 Parameter model of fracturing pump crankshaft set

The aggregate parameter model of the transmission system can be simplified as shown in Fig 5.

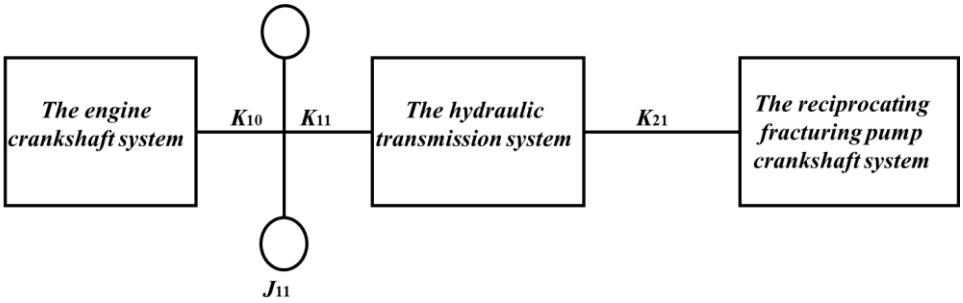

Figure 5 Parameter model of the total set of equipment transmission system on the fracturing truck

The simplified mathematical model expression of the transmission system is shown in Eq (1).

$$\boldsymbol{J}\ddot{\boldsymbol{\theta}} + \boldsymbol{C}\dot{\boldsymbol{\theta}} + \boldsymbol{K}\boldsymbol{\theta} = \boldsymbol{T} \tag{1}$$

2.2 Sensitivity Analysis

In this study, the sensitivity problem is solved based on the direct derivative method, as shown in Eq (2).

$$\lambda \mathbf{J}[A] - \mathbf{K}[A] = \mathbf{0} \tag{2}$$

The physical parameter p (rotational inertia or torsional stiffness) of Eq. (3) is derived by taking the partial derivative and substituting it into Eq. (2). The total set of parameters undamped free vibration satisfies the requirement of vibration orthogonality, and the left multiplication of the above equation yields Eq. (4).

$$2\omega_i \frac{\partial \omega_i}{\partial p}\mathbf{J}\boldsymbol{A}_i + \omega_i^2 \frac{\partial \mathbf{J}}{\partial p}\boldsymbol{A}_i - \frac{\partial \mathbf{K}}{\partial p}\boldsymbol{A}_i = \mathbf{0} \tag{3}$$

$$\frac{\partial \omega_i}{\partial p} = \frac{-\boldsymbol{A}_i^T\left(\omega_i^2 \frac{\partial \mathbf{J}}{\partial p} - \frac{\partial \mathbf{K}}{\partial p}\right)\boldsymbol{A}_i}{2\omega_i} \tag{4}$$

Denote $S(\omega_i \mid p) = \frac{\partial \omega_i}{\partial p}$, when is the sensitivity of the intrinsic frequency with respect to the rotational inertia J_j, as shown in Eq. (5). When $S(\omega_i \mid p)$ is the sensitivity of the intrinsic frequency with respect to the torsional stiffness $\boldsymbol{K}_j$, as shown in Eq. (6).

$$S(\omega_i \mid J_j) = \frac{\partial \omega_i}{\partial J_j} = \frac{-\omega_i^2 \boldsymbol{A}_i^T \frac{\partial \mathbf{J}}{\partial J_j}\boldsymbol{A}_i}{2\omega_i} = \frac{-\omega_i^2 (\boldsymbol{A}_i)_j^2}{2\omega_i} \tag{5}$$

$$S(\omega_i \mid K_j) = \frac{\partial \omega_i}{\partial K_j} = \frac{\boldsymbol{A}_i^T \frac{\partial \mathbf{K}}{\partial K_j} \boldsymbol{A}_i}{2\omega_i} = \frac{[(\boldsymbol{A}_i)_j - (\boldsymbol{A}_i)_{j+1}]^2}{2\omega_i} \quad (6)$$

From Eq. (5) and (6), it can be seen that the sensitivity of the rotational inertia at the inertia disc with larger relative amplitude is higher for the inherent frequency, and the sensitivity of the torsional stiffness at the inertia disc with larger amplitude difference between the two ends is higher for the inherent frequency.

The location with higher sensitivity can be identified and dynamically modified, or the sensitivity of a location can be calculated separately and modified individually. The sensitivity analysis of the first four orders of torsional inherent frequency of the transmission system to each part of the rotational inertia and torsional stiffness can be obtained from the sensitivity of each component as shown in Fig 6 - Fig 9.

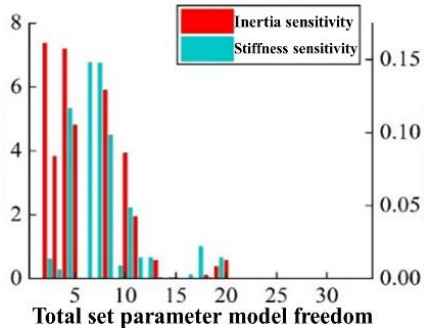

Figure 6 Sensitivity of first order fixed frequency

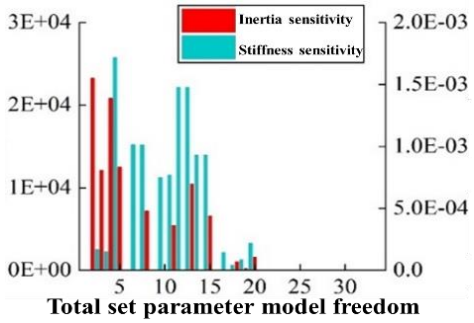

Figure 7 Sensitivity of second order fixed frequency

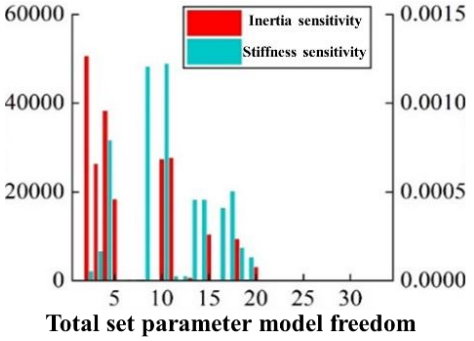

Figure 8 Sensitivity of third order fixed frequency

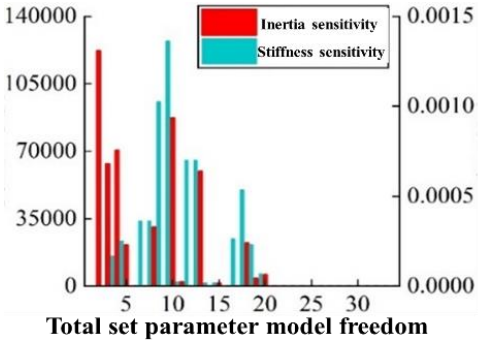

Fig 9 Sensitivity of fourth order fixed frequency

From the above figure, it can be seen that the higher sensitivity parts are at the engine crankshaft and transmission drive shaft. Due to the more complex structure of the engine crankshaft, higher production cost and more influencing factors after modification, structural modification is considered at the higher sensitivity of the transmission drive shaft to change the torsional vibration characteristics of the shaft system. From the above sensitivity analysis, it can be found that after ignoring the first 12 inertia discs where the engine crankshaft is located, the higher sensitivity of rotational inertia and torsional stiffness are at the intermediate drive shaft of transmission gear 1 and gear 2. Therefore, in this study, the dynamics parameters are modified for the intermediate drive shaft in the transmission to achieve the purpose of vibration reduction.

2.3 Design Variables

The structural dimensions of the drive shaft directly affect the torsional stiffness and rotational inertia of the system, which in turn influence the torsional vibration characteristics of the transmission system. Therefore, the optimized design of the key structural dimensions can improve the performance of the transmission system and even the whole machine to a certain extent. The structural dimensions of the

intermediate drive shaft are shown in Fig 10.

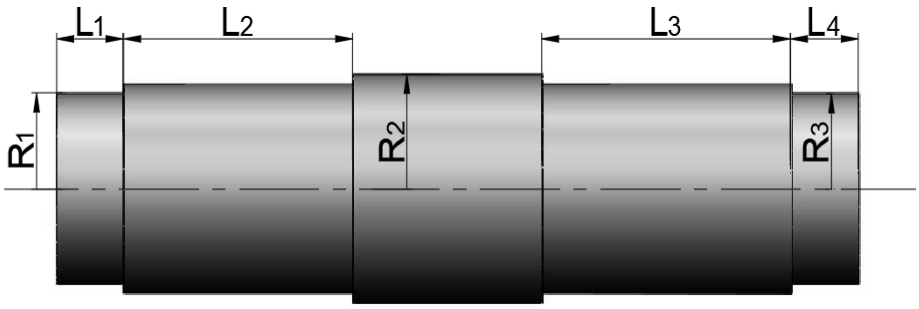

Figure 10 Diagram of optimized dimensions

Due to the fact that the drive shaft needs to be assembled with gears on both sides and the distance between the two gears is fixed, the radius dimensions and shoulder lengths at the journals on both sides cannot be varied. In order to reduce the difficulty of the optimization scheme, the structural dimensions that do not affect the assembly relationship of the system are selected as design variables. The seven parameters of journal radius R_1 and R_3, shoulder radius R_2, and each step length L_1~ L_2 of the intermediate drive shaft were selected as design variables in order to optimize the performance of the drive shaft by reconfiguring these crankshaft structural dimensions that do not affect the assembly relationship of other components.

Table 1 Range of values of design variables

Variables	Initial Value /mm	Constraint range /mm	Variables	Initial Value /mm	Constraint range /mm
R_1	50	45~55	L_2	137	120~150
R_2	60	58~68	L_3	149	134~164
R_3	50	45~52	L_4	40	36~44
L_1	40	36~44			

2.3 Optimization Objectives

The optimization objective of this study is to reduce the maximum torsional amplitude of the engine crankshaft output in one response cycle, the mathematical expression of which shown in Eq (7).

$$\begin{aligned} &min && f_i(x) && i=1,2,\cdots,I \\ &subject\ to && x_i^{(L)} \le x_i \le x_i^{(U)} && i=1,2,\cdots,I \end{aligned} \tag{7}$$

in which, f_i is the maximum torsional amplitude of the engine crankshaft output produced by the *i*-th iteration; I is the maximum number of iterations; x_i is the optimization parameter; $x_i^{(L)}$, $x_i^{(U)}$ are the maximum and minimum values of the optimization parameter, respectively.

3 ACO algorithm and its Improvement

3.1 Design Code Disk

In order to overcome the defects of the traditional ant colony algorithm in the continuous domain optimization problem, a code disk is designed in this study. By setting the number of optimized parameters to *n*, and the parameters are accurate to *L* decimal places, a code space of size 0 ~ 9 is designed, and each column is arranged with ten numbers from 0 ~ 9 in turn, as shown in Fig 11.

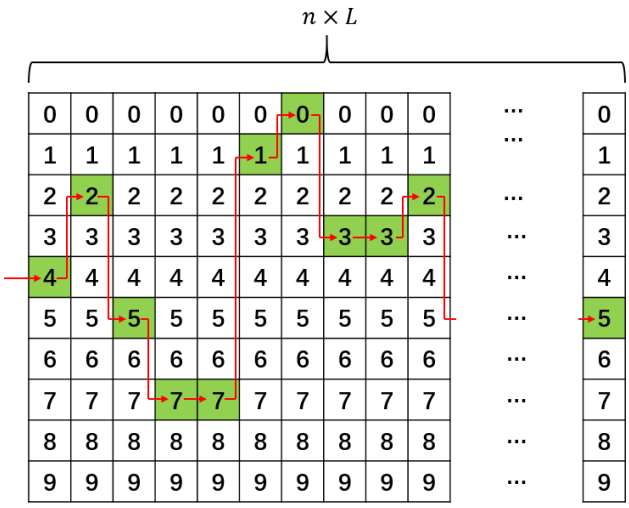

Figure 11 Schematic diagram of the code disk

The ants depart from the left side of the coding disk, taking only one code number per column, and after its passage through the code space, the obtained nL series, denoted as d_j (j=1、2、3…nL), and the parameter taking coefficient Si can be derived from Eq. (8).

$$S_i = \sum_{j=(i-1)L+1}^{iL} (10^{-(j \bmod L)} \times d_j) \tag{8}$$

Based on Eq. (8), the optimization parameters can be expressed as Eq. (9).

$$x_i = (x_{\max}(i) - x_{\min}(i)) s_i + x_{\min}(i) \tag{9}$$

in which: $x_{\max}$ is the maximum value of the optimized parameter and $x_{\min}$ is the minimum value of the optimized parameter. After completing the encoding, the continuous domain optimization problem is transformed into a discrete path finding problem within the encoding disk, which is the strength of ACO.

.

3.2 Improved state transfer strategy and heuristic function

In the ACO algorithm, the ants select the coding number of the next coding column based on the pheromone and heuristic information on the path, and the transfer rule is shown in Eq (10) - Eq (14)

$$S_j = \begin{cases} arg\left(max\left(\tau_{ij}(t)_{i=1,2,\ldots,10}\right)\right) & q \le q_0 \\ S_{pi} & q \ge q_0 \end{cases} \tag{10}$$

$$S_{pi} = find(Pcum(i,j) \ge rand) \tag{11}$$

$$Pcum(i,j) = \sum \left(\frac{P_k(i,j)}{\sum_{k=1}^{10} P_k(i,j)} \right) \tag{12}$$

$$P_k(i,j) = [\tau_{ij}(t)]^{\alpha} [\eta(i,j)]^{\beta} \tag{13}$$

$$\eta(i,j) = \frac{1}{f(k)} \tag{14}$$

in which, S_{pi} returns the independent variable when the function is maximum; $Pcum$ is the node number selected by roulette, is the roulette function, $P_k(i, j)$ is the probability function of the

ant to select the next node, α is the pheromone importance factor; β is the heuristic function importance factor; $\eta(i,j)$ is the heuristic function, is the torsional amplitude of the engine crankshaft output obtained by generating the path after selecting *k* nodes. *k* nodes after the unselected nodes are predicted by roulette method. By using this method, a random set of parameters is generated for heuristic calculation at the beginning of the algorithm execution, while the current optimal parameters are heuristically selected after the pheromone convergence.

3.3 Improved Pheromone Update Rule

When the iteration is completed, the pheromone is added to the current optimal path, and the pheromone is evaporated once for all paths with a maximum-minimum range restriction on the pheromone. The initial pheromone is set to $\tau_{\max}=5$, as shown in Eq (15) - Eq (17).

$$\tau_{ij}(t+1)=(1-\rho)\tau_{ij}(t)+\Delta_{ij} \tag{15}$$

$$\Delta\tau_{ij}=\frac{Q}{f_{best}} \tag{16}$$

$$\tau_{ij}(t)=\begin{cases}\tau_{ij}(t)=\tau_{max} & \tau_{ij}(t)>\tau_{max}\\ \tau_{ij}(t)=\tau_{ij}(t) & else\\ \tau_{ij}(t)=\tau_{min} & \tau_{ij}(t)<\tau_{min}\end{cases} \tag{17}$$

in which: τ_{max} is the maximum value of pheromone; τ_{min} is the minimum value of pheromone, $\tau=\frac{\tau_{\max}}{\rho f_{best}}$, $\tau_{\min}=\frac{t_{\max}}{20}$. The pheromone concentration increment *Q* is the number of pheromones released by ants in a single pass. The larger *Q* is, the stronger the positive feedback of the algorithm and the faster the convergence, while the randomness and global search ability will be weakened. In this study, an adaptive method is used to update the pheromone concentration increment, as shown in Eq (18).

$$Q=e^{-0.7(I-1)/I_{\max}} \tag{18}$$

in which: I is the current number of iterations; $I_{\max}$ is the maximum number of iterations, $I_{\max}=100$.

4 Experimental simulation and analysis

In this study, the traditional ACO and the improved ACO are used to optimize the nonlinear system, and the two algorithms are performed 25 times respectively, and the simulation results are shown in Table 2.

Table 2 Comparison of algorithm optimization results

Comparative items	Traditional ACO	**Improved ACO**
Average number of convergences	63.8	**18.2**
Global optimal solution	0.48748°	**0.48546°**
Number of global optimal solutions	6	**24**
Probability of global convergence	24%	**96%**

From Table 2, it can be seen that the improved ACO algorithm outperforms the traditional ACO algorithm in terms of global optimal solution and convergence speed. The convergence curves obtained using the traditional and improved ACO algorithms are shown in Fig. 12 and Fig. 13, separately, and the pheromone matrices at the end of the algorithm are shown in Fig. 14 and Fig. 15, respectively.

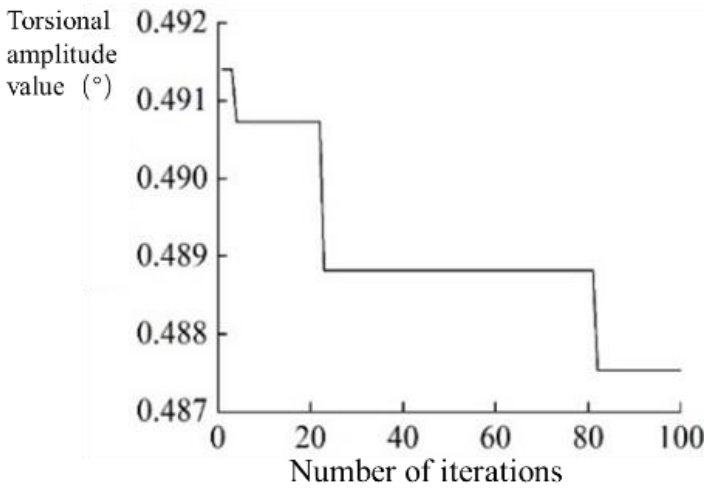

Figure 12 The convergence curve of the traditional ACO

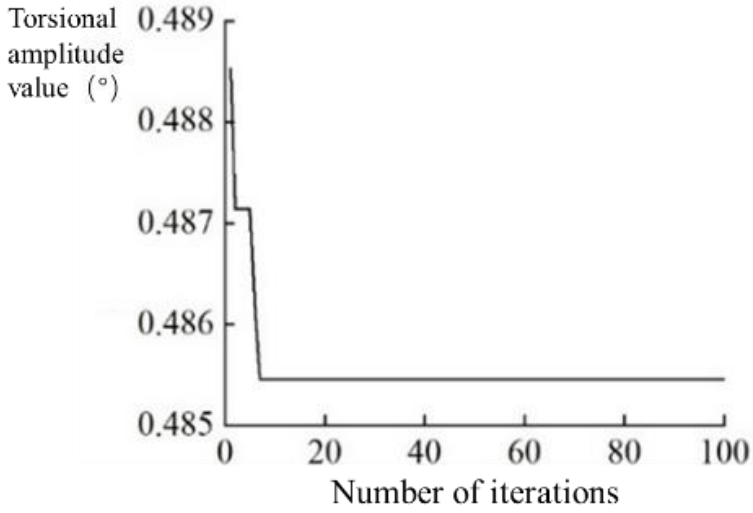

Figure 13 The convergence curve of the improved ACO

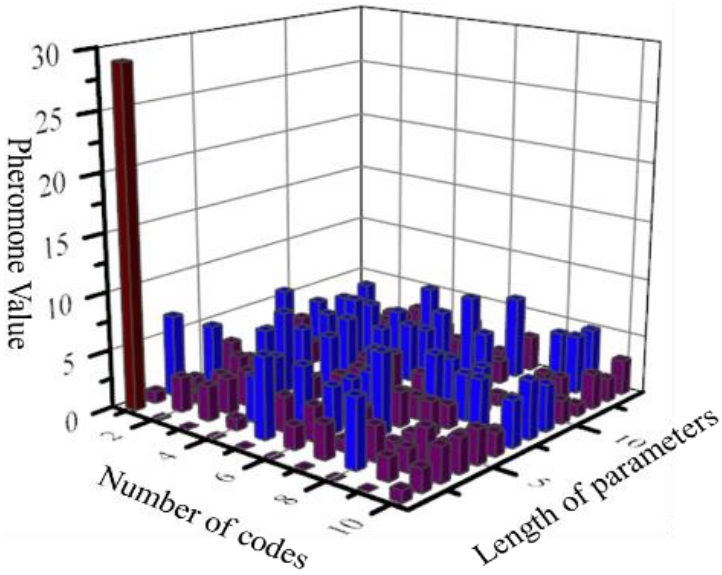

Figure 14 The final pheromone of the traditional ACO

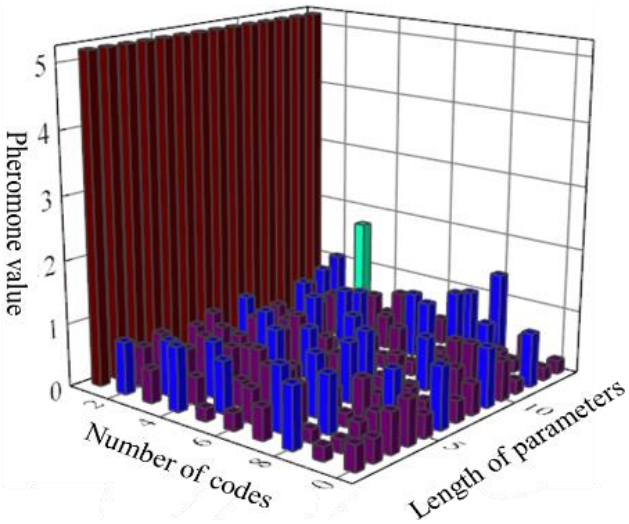

Figure 15 The final pheromone of the improved ACO

From the convergence curve, it can be seen that the traditional ACO algorithm converges after 80 iterations, and the magnitude of the original system decreases by 16.85%, while the improved ACO converges after 7 iterations, and the magnitude of the optimization decreases by 17.19%, which indicates that the traditional ACO algorithm falls into local convergence. From the final pheromone graph, it can be found that the final pheromone of the traditional ACO algorithm does not converge to a path. The final pheromone diagram shows that the pheromone of the traditional ACO does not converge to a path and is irregularly discrete, and the difference between the maximum and minimum pheromone values is large, which is easy to fall into the local optimum. However, the final pheromone of the improved ACO converges to a path, and the difference between the maximum and minimum pheromone values is not large, which still retains a better global search ability in the convergence state. The improved ACO is used for 25 optimizations, in which the best optimization solution is found in 24 times, and only one converges in the middle, and the global convergence rate of the algorithm is 96%. The comparison of the torsional vibration at the output of the engine before and after the improvement is shown in Fig. 16.

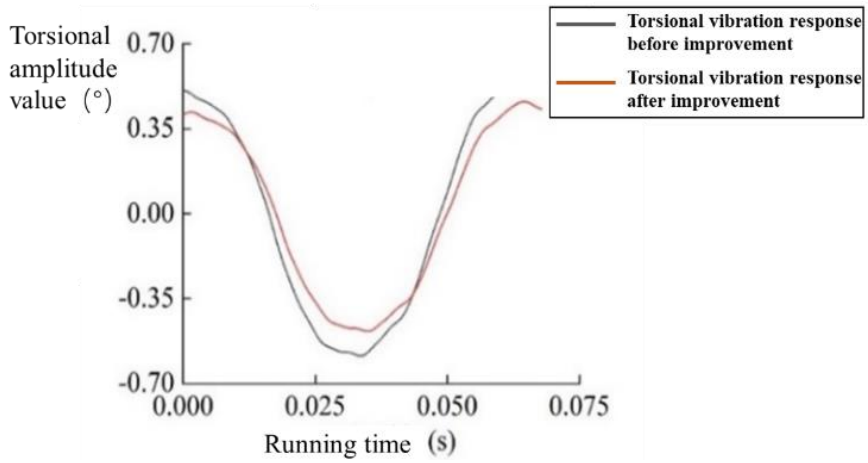

Figure 16 Comparison of torsional vibration response of the traditional and improved ACO

The optimal combination of each key dimension of the structure to be optimized in the drive train of the fracturing truck obtained by using the improved ACO algorithm is [45,58,45,36, 120, 134,36]. Compared with the before and after optimization, the torsional amplitude value of the transmission system of the equipment on the fracturing truck decreased by 17.199%. The maximum torsional amplitude value of the optimized transmission system is 0.48546°, which does not exceed the maximum torsional angle of 0.5° permitted by safety, and the optimization

effect of the improved ACO algorithm is significant, and the optimized transmission system meets the industry standard.

Conclusion

In this study, the torsional vibration optimization of the equipment transmission system on the fracturing truck stage is conducted by the improved ACO algorithm. The traditional ACO algorithm is improved and introduced into the continuous domain optimization problem by adding coding disks to solve the structural size optimization problem. Furthermore, in order to solve the shortcomings of the traditional ACO which is easy to be premature, the parameter design and the improved heuristic function are also proposed to predict the untraveled path of ants according to the pheromone distribution. The improved ACO algorithm is applied to optimize the torsional vibration amplitude of the equipment transmission system on the fracturing truck platform, so that the torsional vibration amplitude of the engine crankshaft output is reduced by 17.199%. Compared with the torsional vibration response of the system before and after the optimization, the results of the improved ACO algorithm are apparent, and the optimized transmission system meets the requirements of operation.

Acknowledgment

This research is funded by “the National Key R&D Program of China” (2021YFB3401400), the Project of Ministry of Industry and Information Technology of the People's Republic of China (CBZ02N23-10).

Reference

1. Fu J, Lai J, Liao G, et al. Genetic algorithm based nonlinear self-tuning fuzzy control for time-varying sinusoidal vibration of a magnetorheological elastomer vibration isolation system[J]. Smart Materials and Structures, 2018, 27(8): 085010.
2. He F, Ye Q. A bearing fault diagnosis method based on wavelet packet transform and convolutional neural network optimized by simulated annealing algorithm[J]. Sensors, 20 22, 22(4): 1410.
3. Hu Z, Yang G. Simulation control model of synchronous motor based on PSO algorithm optimization in power system[J]. Energy Reports, 2022, 8: 1044-1054.
4. Zhou X, Ma H, Gu J, et al. Parameter adaptation-based ant colony optimization with dynamic hybrid mechanism[J]. Engineering Applications of Artificial Intelligence, 2022, 114: 105139.
5. Scenna, F., Anaut, D., Passoni, L.I., et al. Reconfiguration of Electrical Networks by an Ant Colony Optimization Algorithm [J]. IEEE Latin America Transactions, 2013, 11(1):538-544.
6. Dai, X.L., Long, S., Zhang, Z., et al. Mobile Robot Path Planning Based on Ant Colony Algorithm with A* Heuristic Method [J]. Frontiers in Neurorobotics, 2019, 13(15):1-23.
7. Mohajerani, A., Gharavian, D. An ant colony optimization based routing algorithm for extending network lifetime in wireless sensor networks [J]. Wireless Networks, 2015, 22 (8):1-11.
8. Douiri, S.M., Elbernoussi, S. A New Ant Colony Optimization Algorithm for the Lower Bound of Sum Coloring Problem [J]. Journal of Mathematical Modelling & Algorithms, 2012, 11(2):181-192.
9. Joelianto, E., Wiranto, I. An Application of Ant Colony Optimization, Kalman Filter and Artificial Neural Network for Multiple Target Tracking Problems [J]. International Journal of Artificial Intelligence, 2014, 7(11):384-400.
10. Liu, C., Wu, L., Huang, X. D., Xiao, W. S. Improved dynamic adaptive ant colony optimization algorithm to solve pipe routing design [J]. Knowledge-Based Systems, 2022, 237:107846.
11. Wu, L., Huang, X., Cui, J., Liu, C., Xiao, W.S. Modified adaptive ant colony optimization algorithm and its application for solving path planning of mobile robot [J]. Expert Systems with Applications, 215 (2023), Article 119 410.
12. Li, G., Liu, C., Wu, L., Xiao, W.S. A mixing algorithm of ACO and ABC for solving path planning of mobile robot [J]. Applied Soft Computing, 148 (2023), Article 110868.
13. Liu C, Wu L, Li G, et al. AI-based 3D pipe automation layout with enhanced ant colony optimization algorithm[J]. Automation in Construction, 2024, 167: 105689.
14. Liu, C., Wu, L., Xiao, W.X., Li, G.X., Xu, D.P., Guo, J.J., Li, W.T. An improved

heuristic mechanism ant colony optimization algorithm for solving path planning [J]. Knowledge-Based Systems, 271 (2023), Article 110540. https://doi.org/ 10.1016/j .knosys.2023.110540.
15. Liu C, Wu L, Li G, et al. Improved multi-search strategy A* algorithm to solve three-dimensional pipe routing design[J]. Expert Systems with Applications, 2024,240:1223 13.
16. Wu L, Yang Y, Maheshwari M. Strain prediction for critical positions of FPSO under different loading of stored oil using GAIFOA-BP neural network[J]. Marine Structures, 20 20, 72: 102762.
17. Wu L, Mei J, Zhao S. Pipeline damage identification based on an optimized back-propagation neural network improved by whale optimization algorithm[J]. Applied Intelligence, 2023, 53(10): 12937-12954.
18. Wu L, Zhang L, Xiao W S, et al. A novel heuristic algorithm for two-dimensional rectangle packing area minimization problem with central rectangle[J]. Computers & Industrial Engineering, 2016, 102: 208-218.
19. Cui J, Wu L, Huang X, et al. Multi-strategy adaptable ant colony optimization algorithm and its application in robot path planning[J]. Knowledge-Based Systems, 2024,288:111459
20. Xiao W, Wu L, Tian X, et al. Applying a new adaptive genetic algorithm to study the layout of drilling equipment in semisubmersible drilling platforms[J]. Mathematical Problems in Engineering, 2015, 2015(1): 146902.
21. Wu L, Mei J, Zhao S. Pipeline damage identification based on an optimized back-propagation neural network improved by whale optimization algorithm[J]. Applied Intelligence, 2023, 53(10): 12937-12954.
22. Xiao W.S, Li G.X., Liu C., et al. A novel chaotic and neighborhood search-based artificial bee colony algorithm for solving optimization problems [J]. Scientific Reports, 2023, 13(1): 20496.